Biomaterials 59 (2015) 12–20

Contents lists available at ScienceDirect

Biomaterials

journal homepage: www.elsevier.com/locate/biomaterials

Generation of nanovesicles with sliced cellular membrane fragments for exogenous material delivery

Jaewoong Yoon [a, 1], Wonju Jo [a, 1], Dayeong Jeong [b, 2], Junho Kim [b, 2], Hwapyeong Jeong [a, 1], Jaesung Park [a, b, *]

[a] Department of Mechanical Engineering, POSTECH, 77 Cheongam-Ro, Nam-Gu, Pohang, Gyeongbuk 790-784, Republic of Korea
[b] School of Interdisciplinary Bioscience and Bioengineering, POSTECH, 77 Cheongam-Ro, Nam-Gu, Pohang, Gyeongbuk 790-784, Republic of Korea

ARTICLE INFO

Article history:
Received 25 November 2014
Received in revised form
8 April 2015
Accepted 10 April 2015
Available online 15 May 2015

Keywords:
Nanovesicle
Drug delivery
Biomimetic material
Self assembly

ABSTRACT

We propose a microfluidic system that generates nanovesicles (NVs) by slicing living cell membrane with microfabricated 500 nm-thick silicon nitride (Si_xN_y) blades. Living cells were sliced by the blades while flowing through microchannels lined with the blades. Plasma membrane fragments sliced from the cells self-assembled into spherical NVs of ~100–300 nm in diameter. During self-assembly, the plasma membrane fragments enveloped exogenous materials (here, polystyrene latex beads) from the buffer solution. About 30% of beads were encapsulated in NVs, and the generated NVs delivered the encapsulated beads across the plasma membrane of recipient cells, but bare beads could not penetrate the plasma membrane of recipient cells. This result implicates that the NVs generated using the method in this study can encapsulate and deliver exogenous materials to recipient cells, whereas exosomes secreted by cells can deliver only endogenous cellular materials.

1. Introduction

Exogenous material delivery such as drug and gene delivery has wide applications in therapeutics. For these purpose, transmembrane delivery is critical with minimal toxic effect. Recently, exosomes (~30–200 nm vesicles composed of a lipid bilayer) secreted by cells into the extracellular environment, are used as nanocarriers for drugs and nucleic acids due to their low toxicity and nano-scale size [1–8]. Due to these unique characteristics, exosomes have possible therapeutic applications [9–11]. However, utilizing exosomes for research is difficult because they are secreted in extremely small numbers (~0.1 μg from million cells for 24 h) and isolation of exosomes requires a lengthy process that give only a low yield [3,4,12].

Liposomes are synthetic vesicles composed of a lipid bilayer being also used as nanocarriers. Most liposome production methods use organic solvent to form and deposit planar lipid bilayers due to insolubility of lipids in aqueous solution [13]. The planar lipid bilayers are mechanically agitated using extrusion or ultrasound, and broken into small free-standing pieces, which then tend to self-assemble into spherical liposomes to reduce their free energy [14–18]. If the planar lipid bilayers self-assemble in some materials dissolved aqueous solution, the lipid bilayers encapsulate the materials [19–22]. Recently, the liposomes encapsulating materials were demonstrated using microfluidic encapsulation systems [23,24]. Although liposomes have similar morphology to those of cell-secreted exosomes and can encapsulate materials, liposomes have critical drawbacks. The liposome generation procedure requires organic solvents and chemical additives which may not be biocompatible [25–28]. Furthermore, the generated liposomes lack functional membrane proteins which have important functions in initiating signal pathways in recipient cells. Despite these limitations, the liposome generation procedure provides an insight into lipid bilayer self-assembly.

Cellular plasma membranes are also composed of lipid bilayers which have the ability to self-assemble into vesicles. We extruded living cells through micro-sized channels to generate NVs [7,29–31]. The NVs enclose cellular contents from origin cells, such as membrane proteins, cytosolic proteins and RNAs, and can also deliver endogenous RNA into cells [29]. To investigate the effect of NV treatment of cells, we developed a polycarbonate device that

* Corresponding author. Department of Mechanical Engineering, POSTECH, 77 Cheongam-Ro, Nam-Gu, Pohang, Gyeongbuk 790-784, Republic of Korea. Tel.: +82 54 279 5418, +82 54 279 2188; fax: +82 54 279 5899.
E-mail address: jpark@postech.ac.kr (J. Park).
[1] Tel.: +82 54 279 5418; fax: +82 54 279 5899.
[2] Tel.: +82 54 279 2188; fax: +82 54 279 5899.

http://dx.doi.org/10.1016/j.biomaterials.2015.04.028

makes large amount of NVs; ES cellular materials in NVs were delivered into skin fibroblasts, and the treated skin fibroblasts proliferated faster than did non-treated cells [8]. Although the NVs generated by extrusion method were effective in deliver endogenous cellular materials, NVs that can be loaded with exogenous materials such as genetic materials are necessary for extensive applications, and the loading efficiency of exogenous materials are closely related to the process of NV generation. In the previous method, the plasma membranes are attached to the wall of microchannels/micropores, elongated, and suddenly broken down without enough opening to the surround buffer, and the NVs generated using this method is not effective to encapsulate exogenous materials.

In this article, we designed a cell-slicing system to generate NVs from living cells; this method exploits the self-assembly of plasma membrane fragments. An array of 500 nm-thick low-stress silicon nitride (Si_xN_y) blades along microchannels was fabricated to slice the plasma membranes of cells flowing through the device. When sliced from a living cell, a free-standing piece of plasma membrane with intact lipid bilayer structure forms a vesicle that contains cellular contents in the origin cells and exogenous materials. This approach to generating exosome-like NVs will provide a promising strategy for delivery of exogenous drugs and genes.

2. Materials & methods

2.1. Device design and fabrication

The cell-slicing device (Fig. 1) consists of two parts: a silicon substrate with Si_xN_y blades and a polydimethylsiloxane (PDMS) block with lithographed microfluidic channel array (Fig. 1a). The Si_xN_y blades on the silicon substrate are 1 μm long and 500 nm thick and are spaced 23 μm apart (Fig. 1b). The microfluidic channels in the PDMS part are 2.5 mm long, 50 μm high and have four different widths (10, 50, 100, 200 μm) with a fixed total cross section (8×10^{-8} m^2); these dimensions were decided because the embryonic stem (ES) cells (~5 μm diameter) clogged the microchannels when the channel height is less than 10 μm. In contrast, the NV generation yield decreased with the elevated height. After aligning and assembling the silicon substrate and the PDMS block, the Si_xN_y blades are perpendicularly aligned in the middle of the PDMS channel array to slice the plasma membranes of incoming cells.

The device was fabricated using conventional bulk silicon fabrication processes and soft lithography. The cantilever-blades were fabricated from Si_xN_y. First, a 100 nm thick silicon oxide (SiO_2) layer was thermally grown and a 500 nm thick Si_xN_y layer was deposited on a (100) silicon wafer by low pressure chemical vapor deposition. For low-stress nitride deposition, SiH_2Cl_2 gas (100 ccm) was used more than NH_3 gas (40 ccm), so the Si/N ratio was estimated as 1.1 [32]. On the wafer, the pattern for Si_xN_y cantilevers was formed by a lithography process using AZ-4330 photoresist. The patterned Si_xN_y layer on the wafer was over-etched using inductively-coupled plasma reaction-ion-etching to develop the pattern on the layer. The SiO_2 layer exposed through the dry-etched Si_xN_y layer was removed by buffered oxide etching to expose single-crystal silicon substrate. The silicon wafer was anisotropically wet-etched using 40% KOH at 70 °C for 1 h.

The pattern for microfluidic channels in the PDMS part was fabricated using soft lithography. SU-8 2100 was spun with 50 μm thickness and lithographically patterned to form the microfluidic channel array, an inlet chamber and an outlet chamber (Fig. 1a). The wafer with the SU-8 pattern was used as a master for the PDMS mold. A mixture of nine parts PDMS silicon elastomer base and one part curing agent was cured at 65 °C for 2 h after bubbles in the mixture were removed. The cured PDMS part was aligned and bonded to the silicon part by oxygen plasma treatment, then baked on a hotplate at 150 °C for 2 h to achieve strong bonding. After connecting tubes to the inlet and outlet port of the device, the assembled apparatus was washed by passing 75% ethanol and deionized water sequentially through the tubes.

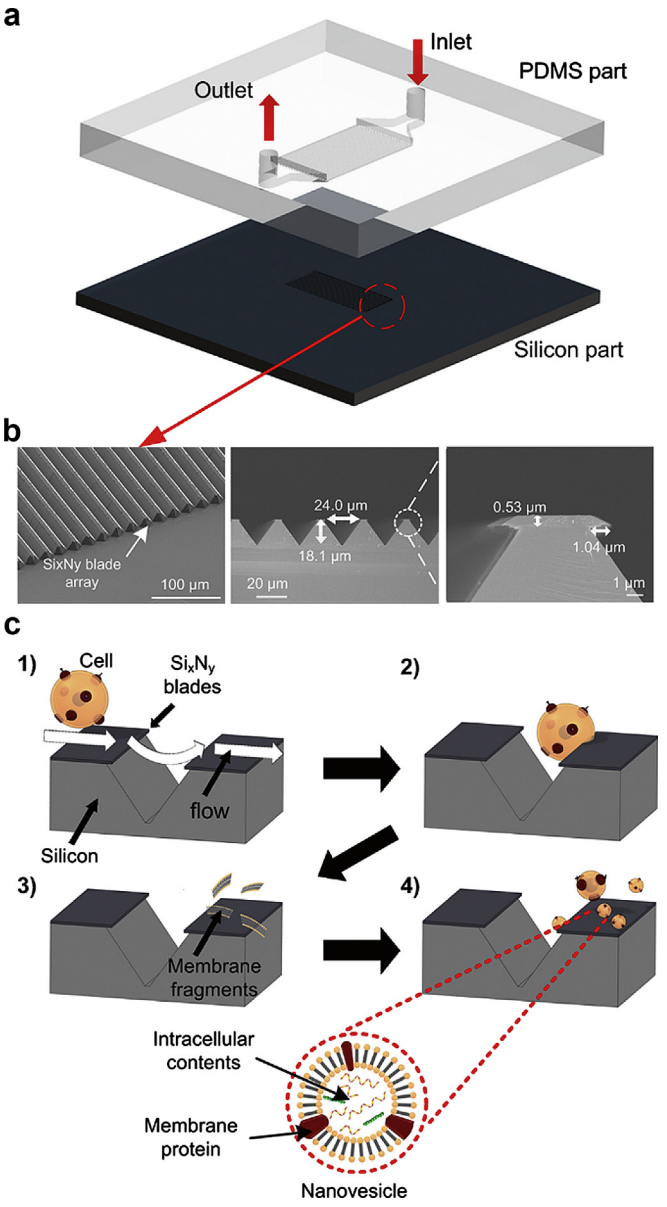

Fig. 1. (a) Schematic structure of cell-slicing device. It is composed of the silicon part with 500 nm-thick Si_xN_y cantilever-blades and the PDMS part with microchannels and an inlet port and an outlet port. (b) The silicon part has parallel Si_xN_y cantilever-blades which have 1 μm-long protrusion and 500 nm-thickness. (c) A schematic of NVs generation by slicing cells. As cells flowed through microchannels, 1) the cells moved down and up due to the flow at the groove and 2) the cells were sliced by Si_xN_y blades 3) into plasma membrane fragments. 4) The plasma membrane fragments self-assembled into small NVs, which were collected along with unsliced cells and cell debris at the outlet.

2.2. Cell slicing in microchannel

Living cells were entrained in the flowing medium and plasma membrane of the cells were sliced when they touched the edge of a cantilever-blade (Fig. 1c). The cross section of a microchannel in

PDMS part is 50 μm × (10, 50, 100 or 200 μm) and the length is 2.5 mm with 75 cantilever-blades in series.

2.3. Study of plasma membrane fragment self-assembly

After the plasma membrane were fragmented, they spontaneously self-assembled in the aqueous phase to form NVs (Fig. 2a). By the second law of thermodynamics, the excess Gibbs free energy of the vesicle is

$$dG = -SdT + VdP + dE_b + dE_l \tag{1}$$

where S is entropy, T is temperature, V is volume, P is pressure, E_b is the bending free energy and E_l is the contour free energy [33,34]. If we assume that 1) the fragments sliced from plasma membranes are planar lipid bilayers, 2) the fragments consist only of phospholipids and 3) T and P are constant, then the excess Gibbs free energy of the vesicle is just the sum of E_b and E_l. For simplicity, if only planar and spherical shapes are considered, the standard bending free energy per unit area e_b of the lipid bilayer membrane is

$$e_b = \frac{dE_b}{dA} = \frac{\kappa}{2}(c_1 + c_2)^2 - \kappa c_0(c_1 + c_2) + \overline{\kappa} c_1 c_2 \tag{2}$$

where κ is the bending rigidity and $\overline{\kappa}$ is the bending modulus [14]. The principal curvatures c_1 and c_2 are identical in this analysis. The spontaneous curvature c_0 is zero because the lipid bilayer is assumed to be symmetric. The contour free energy per unit length E_l is

$$E_l = \frac{dE_l}{dl} = \gamma \tag{3}$$

where γ is the edge tension [34]. Then, the total Gibbs free energy simplifies to

$$G(\theta) = \int e_b dA + \int e_l dl = 2\pi\kappa_b[1 - \cos(\theta)] + 2\gamma(\pi A)^{0.5} \sin\left(\frac{\theta}{2}\right) \tag{4}$$

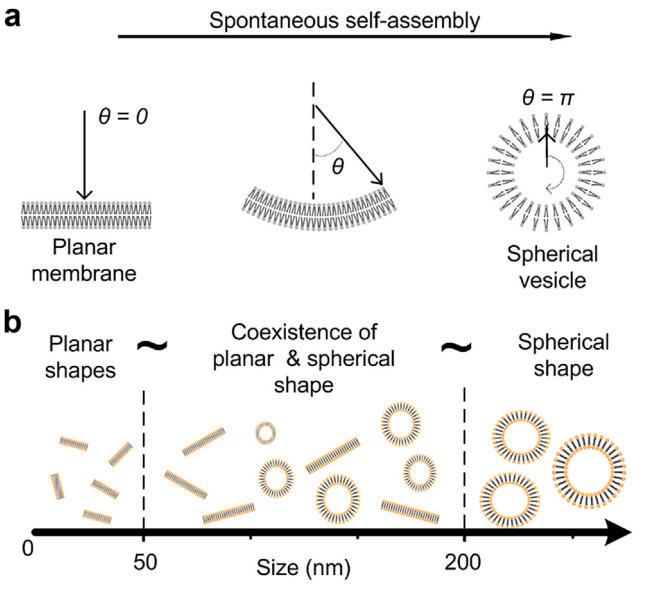

Fig. 2. (a) A schematic representation of spontaneous self-assembly from planar membrane. (b) Stable shape of lipid bilayer along with size according to minimum free energy.

in terms of the angle θ (Fig. 2a), where $A = 2\pi r^2[1 + \cos(\theta)]$ is the area of the membrane and $l = 2\pi r \sin(\theta)$ is its contour length. The radius r of the sphere is the inverse of the principal curvature, and $\kappa_b = 2\kappa + \overline{\kappa}$. To analyze parameters, the Gibbs free energy is converted into dimensionless form

$$\overline{G}(\theta) = \frac{G}{2\pi\kappa_b} = 1 - \cos(\theta) + \alpha \sin\left(\frac{\theta}{2}\right) \tag{5}$$

where $\alpha = (\gamma/\kappa_b)(A/\pi)^{0.5}$ determines whether the planar or spherical shape is more stable (has minimum free energy). When $\alpha < 2$, the planar shape has the minimum free energy; when $\alpha > 4$, the spherical shape has the minimum free energy. However, when $2 \leq \alpha \leq 4$, energy is needed to change the shape. By using reasonable values of κ_b and γ, the information about the effects of α can be used to identify which geometry is the most stable along with the radius of the sphere. The empirical values are $\kappa_b \sim 5$–$25\ k_bT$ and $\gamma \sim 1$–$2\ k_bT/l$, where k_b is the Boltzmann constant [33,35]; *i.e.*, both planar and spherical lipid bilayers ranging from 50 nm to 200 nm are stable and must overcome an energy barrier to change shape; lipid bilayers > 200 nm should be spherical (Fig. 2b). Therefore, vesicles >50 nm may be considered stable in the aqueous phase when they are spherical.

2.4. Cell culture

Murine embryonic stem cells (ES-D3; ATCC, Manassas, VA) were maintained in knockout DMEM (Gibco) including 15% replacement fetal bovine serum (FBS, Gibco), 4 mM L-glutamine (Sigma), 100 μg mL^{-1} penicillin-streptomycin (Gibco), 10 ng mL^{-1} leukemia inhibitory factor (ORF genetics) and 0.1 mM 2-Mercaptoethanol (Sigma).

NIH 3T3 (ATCC, CRL-1658) cells were maintained in DMEM (Hyclone) including 10% FBS (Hyclone) and 100 μg mL^{-1} penicillin-streptomycin (Gibco). Proteins and RNAs in NIH 3T3 cells were isolated and used as negative controls of experiments for characterization of NV contents.

Mouse embryonic fibroblasts expressed green fluorescent protein (MEF-GFP) were isolated from C57BL/6-Tg(ACTB-EGFP)10sb/J mice using a slightly modified protocol [36]. The isolation from C57BL/6-Tg(ACTB-EGFP)10sb/J mouse was approved by the Institutional Animal Care and Use Committee at POSTECH, Pohang, Republic of Korea (approval number: 2013-01-0016). MEF-GFP cells were maintained in DMEM including 10% FBS and 100 μg mL^{-1} penicillin-streptomycin (Gibco).

2.5. NV generation and isolation

The ES cells were suspended to 1×10^7 cells mL^{-1} with PBS buffer. The cell-suspension buffer (1 mL) was loaded in a 1 mL disposable syringe. The syringe was connected to the inlet of the microchannels; another syringe was connected to the outlet of the microchannel to collect the sample. The cell-suspension buffer was passed 11 times through the device with hand (~1 mL/min) at 4 °C. The sample from the outlet was pre-cleaned by centrifugation at 210 g-force for 15 min to eliminate unsliced cells. The supernatant was loaded on a 10%–30% (weight/volume percent of iodixanol) Opti-prep gradient solution in an ultracentrifuge tube. The tube was centrifuged at 100,000 g-force for 1 h at 4 °C to separate the NVs from cell debris. The entire band between 10% and 30% Opti-prep was collected and used in the following assays.

NVs could also be generated from plasma membrane fragments caused by shear force instead of by slicing while they pass through the device [29], or by natural exosome secretion by the cells [4–6,11]. To quantify these effects, the above two tests were

repeated on samples that had been passed through a device that had neither cantilever blades nor grooves (shear stress rupture) but was otherwise identical to the test device, and on samples of buffer containing cells that had been stored at 4 °C for 6 h (exosome secretion).

To confirm the effect of flow rate on the NV generation efficiency, ES cell-suspension buffer was passed 11 times through the 200 μm-wide-channel using a syringe pump with 50, 100, 200 μl/min at 4 °C. The samples from the outlet were collected and done with equivalent NV isolation process.

2.6. NV size analysis and quantification

The quantity of isolated NVs was estimated using a Bradford protein assay (Bio-Rad Laboratories) to measure the surface proteins tethered on the membrane of NVs [1,4]. The numbers and sizes of particles were measured using a nanoparticle tracking assay (NTA, Nanosight, Nanosight LM10-HS system). Concentrated sample was diluted to 0.5 μg mL^{-1} with PBS. Samples (1 mL) were loaded on a stage after cleaning it with HEPES buffered saline buffer. Each sample was measured three times.

The size distributions of NV generated from each of the 10, 50, 100 and 200 μm-wide-channels were measured using a dynamic laser scattering (DLS) instrument (Zetasizer 3000HSA, Malvern Instrument). A 1 mL sample of NVs was quantified and adjusted to a concentration of 5 μg mL^{-1} for measurement. Morphology and size of the NVs were examined using a transmission electron microscope (TEM, Joel 10011, Japan). A 5 μL sample was loaded on the Formavar carbon film (Electron Microscopy Science) for 10 s and removed using filter paper. Then 7 μL of 2% uranyl acetate was loaded on the grid for 10 s and the residue was removed using filter paper. The grid was completely dried for 30 min at room temperature under filter paper. The following tests were conducted for NVs from 50, 100 and 200 μm-wide-channels only, because generation of NVs with 10 μm-wide-channels required too much time due to low flow rate.

2.7. Characterization of NV contents

Protein content of each sample (ES-D3, NIH-3T3, NVs) was measured by extracting proteins using a mixture of RIPA buffer and protease inhibitors for 10 min. The samples were centrifuged at 10,000 g-force for 10 min and the supernatants were collected in different tubes. The protein concentration was measured using a BCA protein assay kit (Thermo scientific). The isolated proteins were used as samples for western blotting to confirm intercellular proteins and membrane proteins.

RNA of each sample (ES-D3, NIH-3T3, NVs) was quantified using spectrophotometry and reverse transcription polymerase chain reaction (RT-PCR). To prepare the samples for analysis, they were lysed using TRI reagent (Sigma) and incubated for 5 min in room temperature. The mixture was mixed with chloroform (Sigma) and centrifuged at 13,500 g-force for 10 min to separate the organic phase from the aqueous phase. As much of the aqueous phase as possible was collected and mixed with the same volume of IPA (Sigma). The sample was stored at −20 °C for 20 min, then centrifuged at 13,500 g-force for 10 min. The supernatant was carefully removed to avoid breaking the RNA pellet. Then the remaining IPA was removed by rinsing in 75% ethanol and centrifuged at 13,500 g-force for 10 min. The ethanol was removed and the pellet was totally dried. The RNA pellet was dissolved in nuclease-free water (Ambion) and the RNA concentration was measured using a spectrophotometer (GENOVA).

Western blotting was performed to confirm the existence of characteristic proteins in NVs. Isolated proteins (5 μg) from NVs were mixed with 5× loading dye, then denatured proteins were separated in 10% SDS-PAGE gel at 120 V for 2 h. The proteins were transferred to polyvinylidene fluoride membrane at 390 mA for 2 h. The membrane was blocked using 5% non-fat dry milk in PBS. Primary antibodies in 5% non-fat dry milk were incubated with the membrane overnight at 4 °C. After washing the membrane three times with 0.05% tween 20 in TBS, second antibodies were also incubated with the membrane for 1 h at room temperature. The targeted proteins were visualized using a chemiluminescent substrate. The antibodies used were: Anti-actin (Santa Cruz), Anti-ICAM-1 (biorbyt), Anti-nanog (Milipore), anti-mouse HRP (Santa cruz) and Anti-rabbit HRP (Santa cruz). Primary antibodies were diluted 1:1000 and secondary antibodies were diluted 1:5000.

The isolated RNA was used as the sample for RT-PCR to confirm the existence of RNA in NVs. Complementary DNA (cDNA) transcripts were obtained using a reverse transcription kit from 1 μg of RNA. Reverse transcription was performed at 42 °C for 70 min and 70 °C for 15 min. Actin (200 bp), Oct 3/4 (100 bp) and Nanog (400 bp) sequences were amplified with the following primers.

Actin	Forward	ACGTTGACATCCGTAAAGAC
	Reverse	GCAGTAATCTCCTTCTGCAT
Oct 3/4	Forward	AGACCATGTTTCTGAAGTGC
	Reverse	GAACCATACTCGAACCACAT
Nanog	Forward	AGGGTCTGCTACTGAGATGCTCTG
	Reverse	CAACCACTGGTTTTTCTGCCACCG

PCR was performed in tubes containing 2 μL of the cDNA and 48 μL of a master mixture. The PCR conditions consisted of 1) denaturation at 94 °C for 2 min, 2) 32 cycles of amplification at 94 °C for 30 s each, 52 °C for 1 min and 72 °C for 1 min and 3) extension at 70 °C for 5 min. For analysis of the PCR products, each sample was run on a 2% agarose gel (30 min, 100 mV), stained with SYBR® Green (molecularprobe) for 10 min then photographed using a BioDoc-It imaging system (UVP).

2.8. Delivery of fluorescent polystyrene beads and confocal microscopy

To assess whether the NVs can encapsulate and deliver exogenous materials into cells, the device was used to generate NVs that contained red fluorescent (RF) polystyrene (PS) beads (22 nm in diameter, Thermo scientific). Stoke's diameters of potential exogenous materials are RNAs, DNAs, proteins and plasmids, usually smaller than 20 nm or approximately 20 nm. In term of size, 22 nm PS bead was used as an indicator for the encapsulating ability of NVs. Additionally, the fluorescent intensity of the polystyrene bead standard was directly proportional to bead concentration, which can give more accurate evaluation of encapsulation efficiency.

To encapsulate beads within NVs, bead suspensions (0.3 mL of 0.1% solids) were diluted in ES cell suspension (1×10^7 cells in 1 mL PBS) which was then passed through the cell-slicing microchannels. To isolate the bead-encapsulating NVs, the sample from the outlet was pre-cleaned, loaded on a 10%–30% Opti-prep gradient solution in an ultracentrifuge tube, and then centrifuged at 100,000 g for 1 h. The entire band between 10% and 30% Opti-prep concentrations was collected and diluted to have the initial volume (1.3 mL). Encapsulation efficiency (EE) of red fluorescent beads in NVs was determined using fluorescent intensity measured by a plate reader (BECKMAN COULTER). EE was defined as $100(I_e/I_t)$, where I_t is the total red fluorescent intensity of the origin bead solution and I_e is the intensity of samples collected after ultracentrifugation.

To correct for the effect of aggregation between beads and NVs, bead-aggregated NVs were generated and the EE was determined. The ES cell suspension (1×10^7 cells in 1 mL PBS) from the outlet of the microchannels was mixed with bead solutions (0.3 mL of 0.1% solids) and the bead-aggregated NVs in mixture were isolated using the equivalent isolation process.

To evaluate whether NVs can deliver exogenous materials into cells, MEF-GFP cells were treated with bare beads, bead-encapsulating NVs and bead-aggregated NVs. MEF-GFP cells (3.5×10^4 cells) were seeded on a 0.2%-gelatin-coated confocal dish (SPL). The bead-encapsulating NVs (10 μg) and bead-aggregated NVs (10 μg) were diluted in cultured media and the bead solutions were also diluted to have equivalent red fluorescent intensity of bead-aggregated NVs. Twelve hours after seeding, the MEF-GFP cells were incubated in the media for 6 h. The samples were fixed and dyed with Hoechst (Sigma), then photographed using a confocal microscopy (Carl Zeiss, LSM 510 Meta).

3. Results & discussion

3.1. NV generation

When the cell suspension buffer flows through the device (Fig. 1c), (1) the cells run down and up due to the groove geometry and (2) touch the blade which is sharp enough to slice the plasma membrane [37]. (3) The plasma membranes are sliced to planar fragments. If the size are less the 50 nm, the planar shape remained planar (Fig. 2b). Meanwhile, if the size are larger than 50 nm, (4) the planar fragments start to self-assembled into NVs, depending on their size, as explained in Materials and Methods. The samples from the outlet were collected and NVs were separated from the unsliced cells and cellular debris after several isolation processes described in Materials & Methods. The diameters of NVs were measured using DLS and the membrane structures were observed in TEM images (Fig. 3).

The size distribution of NVs from 10 μm-wide-channels had a peak at ~90 nm, but the distribution of 50 and 100 μm-wide-channels had the same peak at ~100 nm (Fig. 3a). The diameter of NVs from 200 μm-wide channels had a peak at ~300 nm. The mean diameters of NVs from 10, 50, 100 and 200 μm-wide-channels were 99 ± 19.18, 123 ± 28.11, 143 ± 50.59 and 307 ± 76.66 nm, respectively (Fig. 3b). The widths of the NV peaks increase as the channel width increased. At all channel widths, the NVs had enclosed spherical membrane structures (Fig. 3c). The TEM images showed a similar size tendency as the DLS data. The results indicate the diameter of NVs increased, as the width of microchannels increased.

The relationship between the channel size and vesicles size may come from the length of sliced membrane fragments. The channel size is proportional to Reynolds number (*Re*), ratio of inertial force to viscous force. In these rectangular channels, *Re* is proportional to hydraulic diameter, $2 \times (50\ \mu m \times \text{width})/(50\ \mu m + \text{width})$. The hydraulic diameter increases as width increases, which means higher inertial force, and increases the impulse with the blades. So the plasma membranes will be larger sliced and self-assembled to bigger NVs.

3.2. Quantification of NVs

The mean protein amount and quantity of NVs generated from 1 million ES cells were measured as ~20 μg and $\sim 150 \times 10^8$ particles, respectively (Fig. 4a,b); The amount of NVs based on Bradford protein assay was ~100 times larger than the amount of exosomes from same number of cells [4]. In detail, the amounts of proteins of NVs from 50 to 100 μm-wide-channels were lower than the amount of protein of NVs from 200 μm-wide-channels, but the number of NVs was similar. The result may occur because the amount of proteins in an equivalent number of NVs would increase as the size of NVs increase; therefore, quantifying the amount of protein to determine the quantity of NVs is only valid when the NVs are of same size.

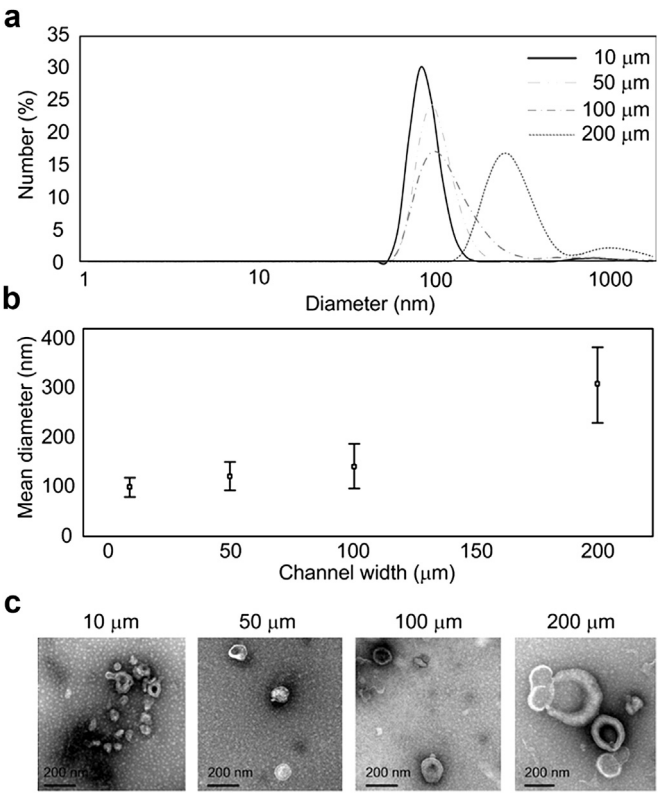

Fig. 3. NVs from cell-slicing device have spherical membrane structure of ~100–300 nm in diameter. (a) Size distribution and (b) mean diameters of the samples from three microchannel width (10, 50, 100 and 200 μm) measured using DLS with equivalent protein amount. (c) TEM images of the samples.

In the controls, the amount of proteins in NVs produced as a result of cell disruption by shear forces using a flat surface device [29] was ~1/8 times that produced by cell slicing. The number of particles produced by shear stress was ~1/7 times the number of particles produced by cell slicing. Also, the amount of proteins in exosomes secreted by cells stored at 4 °C during the experiment was negligible compared with those in generated NVs [3,4,12]. These results demonstrate that the cell-slicing microdevice can generate NVs using Si_xN_y blades and that the main cause of vesicle generation is the presence of the blades, not the shear stress by shear force by channel wall.

The effect of flow rate on NV generation efficiency was confirmed using NTA (Fig. 4c). When flow rate was 50 and 100 μl/min, the number of NVs was $(180 \pm 10.0) \times 10^8$ and $(191 \pm 5.57) \times 10^8$. When the flow rate increased to 200 μl/min, the number of NVs was decreased to $(137 \pm 26.9) \times 10^8$. Meanwhile, protein amounts by Bradford assay showed that higher flow rate provided more membrane proteins (data not shown). These results indicate that as flow rates increase, the sizes of NVs will increase.

3.3. Quantification of NV components

The quantities of total proteins and RNAs in the NVs increased linearly with the quantity of generated NVs, as is observed in exosome quantification [38,39]. For quantitative evaluation of the NV generation by the device, total proteins and total RNAs in NVs

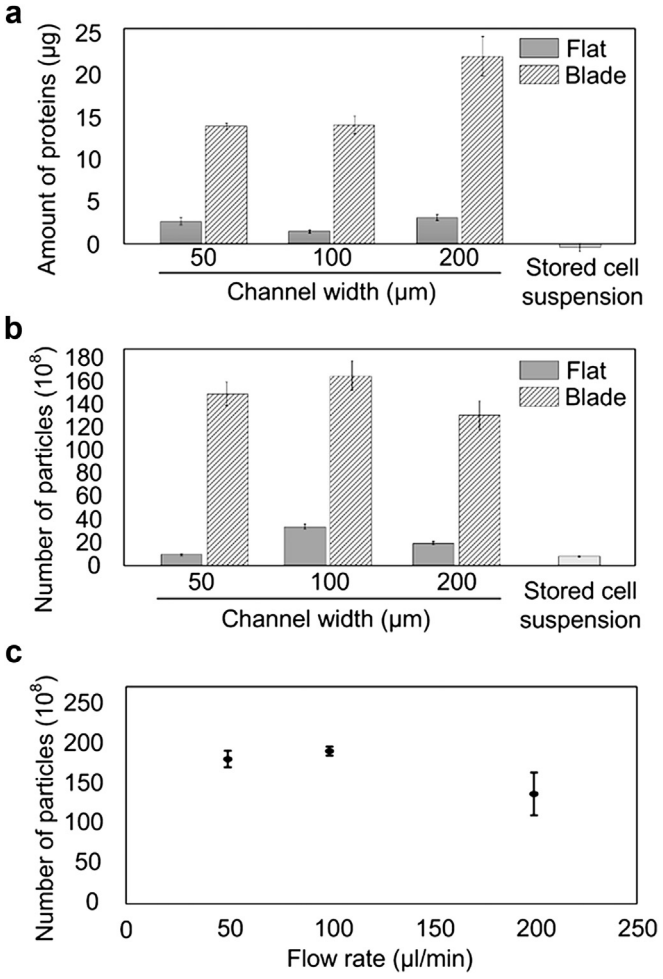

Fig. 4. Samples from different condition were compared: Flat; flowing through the microchannel with flat surface, Blade; flowing through the microchannels with cantilever-blades and Stored cell suspension; just storing at 4 °C for 6 h. (a) Protein amount of the samples from 1 million ES cells was measured with the Bradford protein assay after several purification steps. (b) NTA measurements of the number of particles of the samples from 10^6 ES cells. (c) NTA measurements of the number of particles of samples according to flow rate from 10^6 ES cells. The data were displayed mean ± SD (n = 3, respectively).

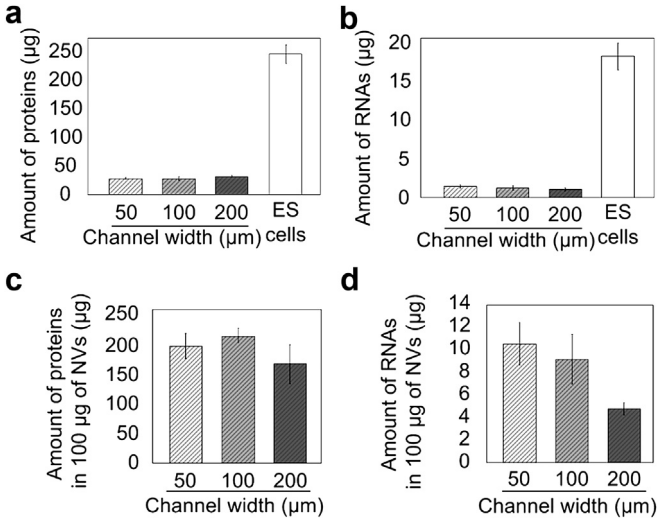

Fig. 5. (a) Total protein and (b) RNA amount in 10^6 ES cells and NVs from the equivalent ES cells. (c) Isolated protein and (d) RNA amount in 100 μg of NVs. The data were displayed mean ± SD (n = 3, respectively).

were measured and compared with those from an equivalent number of ES cells used in NV generation. The width of the microchannel had little effect on the amount of protein or RNA in the NV membranes produced from 1×10^6 ES cells. The total protein in NVs from 1×10^6 ES cells (~30 μg) was ~1/8 of the amount of protein isolated from the same number of ES cells (~250 μg, Fig. 5a). The total RNAs in NVs from 1×10^6 ES cells (~1.5 μg) was ~1/12 of the RNAs isolated from the same number of ES cells (~18 μg, Fig. 5b). The result reveals that ~1/10 of ES cell components were enveloped in the membrane of NVs.

The concentration of proteins and RNAs in equivalent amount of NVs was measured. Total protein quantity in 100 μg of NVs was measured as ~195 μg using BCA assay. The width of the microchannel had no consistent effect on protein concentration (Fig. 5c), but RNA concentration decreased from 10.5 μg in 50 nm-wide microchannel to 4.79 μg in 200 nm-wide microchannel (Fig. 5d).

3.4. Components of NVs

The NVs were generated from fragments of sliced ES cells, so the NVs are expected to have cellular contents such as a lipid bilayer membrane, membrane proteins and intracellular proteins and RNAs. Oct 3/4 was used as the representative marker of ES cells, and ICAM-1 was used as a marker of plasma membrane protein [40,41]; they were observed in samples from ES cell and in generated vesicles (Fig. 6a). This observation indicates that the NVs include membrane protein and that the lipid bilayer membrane of the vesicle was directly derived from the plasma membrane of the cell. Oct 3/4 and β-actin are intracellular proteins in ES cells; these proteins were detected in samples from ES cells and NVs; therefore the NVs contain both membrane proteins and intracellular proteins from the lipid bilayer membrane of the original ES cells.

RT-PCR detected Oct 3/4, Nanog and β-actin mRNAs in ES cells and NVs (Fig. 6b). This reveals that the NVs enclose intracellular RNAs from ES cells. The RNA profile for ES cells had three peaks (small RNA and two rRNA); the RNA profile for all NVs also had three peaks that correspond to the ES cell RNA profile (Fig. 6c). These results show that the NVs were composed of cellular components (membrane proteins, intracellular proteins and mRNAs) from the original ES cells. The presence of miRNA, rRNA and tRNA suggests that the NVs can be used as vehicles for RNA delivery.

3.5. Exogenous material encapsulation efficiency

The bead-encapsulation efficiency of NVs was assessed by measuring fluorescence intensity. Bead-encapsulating NVs were generated by flowing ES cell suspension mixed with RF beads solution through the cell-slicing system. During the process, the beads could be encapsulated in NVs, aggregated to the lipid membrane of NVs or remained without any interaction with NVs. After the sample was isolated by using gradient ultracentrifugation (Fig. 7a), the EE of the sample was measured ~60% (Fig. 7b). The contribution to the EE of all of these cases need to be considered for accurate evaluation of the EEs.

First, the bare beads cannot exist in the layer of the discontinuous density gradient (10–30%) by themselves due to the density, the beads in the layer were only inside the NVs (encapsulating) or outside the NVs (aggregated). Accordingly, the contribution of the bare bead to the EE after the equivalent gradient centrifugation was just few percent, and may be negligible (Fig. 7b). Therefore, only the EE from bead-encapsulating NVs and bead-aggregated NVs need to be considered. To measure the EE of the bead-aggregated NVs, the

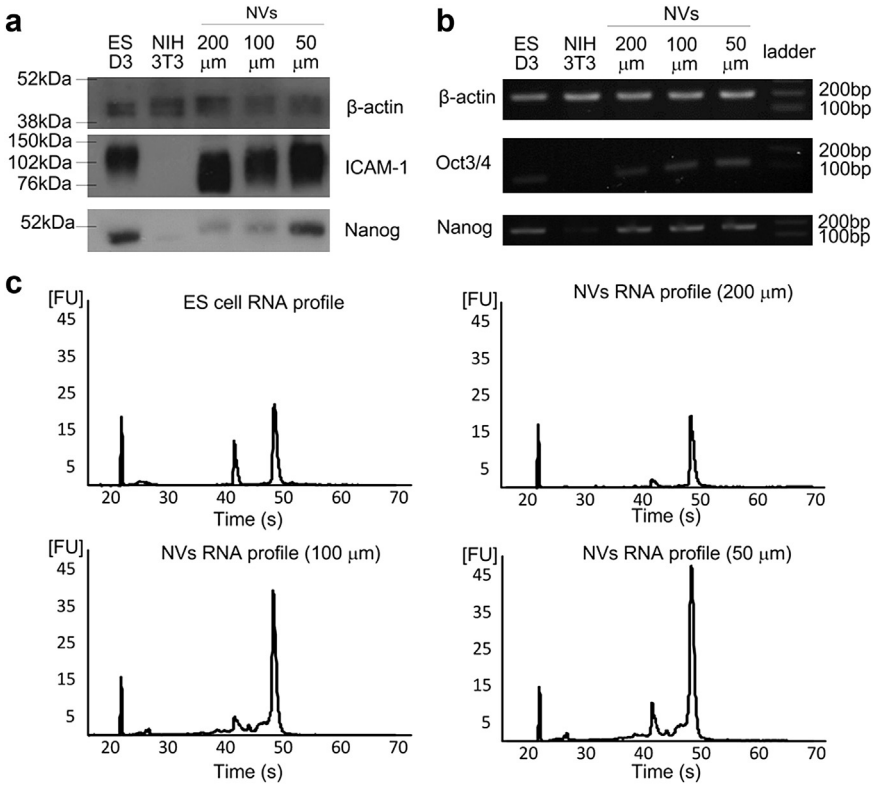

Fig. 6. (a) Western blotting of ES cell proteins using ICAM-1, Nanog and Oct3/4. (b) RT-PCR for ES cells, NIH-3T3 fibroblast and NVs from ES cells. (c) RNA profiles from Bioanalyzer™ for ES cells and NVs.

bead-aggregated NVs need to be separated from the sample. However, this separation is difficult, and the bead-aggregated NVs was separately generated by mixing bare bead and NVs as described in Materials and Methods (Fig. 7a). Then, the bead-aggregated NVs were isolated in the same way, and the EE of bead-aggregated NVs was measured about ~30% (Fig. 7b). Therefore, the corrected EE of bead-encapsulating NVs was estimated as ~30% by subtracting the EE of the bead-aggregated NVs from the EE of the sample generated by flowing ES cell suspension mixed with RF beads solution through the cell-slicing system.

In addition to aggregation, the fluorescent intensity can be originated from lipid monolayer coated beads which could potentially be isolated due to density change. To rule out the possibility, the size distribution of bead-encapsulating NVs, bead-aggregated NVs generated with 200 μm wide channel, and 22 nm beads were measured using DLS (Fig. 7c). Beads had sharp peak at 22 nm. The bead-encapsulating NVs had similar size distribution with NVs. If there are bead surrounded with lipid monolayer, peaks below the 100 nm should exists. No peak around 100 nm in size distribution of bead-encapsulating NVs suggests that there are no beads outside the membrane of NVs. However, size distribution of bead-aggregated NVs had two peaks at ~100 nm and 600 nm, which means there are many beads outside the membrane of NVs. The result reveals that the sliced plasma membrane fragments can encapsulate ~30% of materials in surrounded buffer when the fragments are self-assembled into NVs. For comparison, the NVs that encapsulated RF beads were generated using extrusion method and isolated using the same process [7]. The fluorescent intensity of the NVs was just ~35%, which is similar to that of the bead-aggregated NVs (Fig. 7b). This result indicates that the NVs generated by extrusion may not encapsulate the beads effectively.

There is a possibility that the detergent in PS bead solution may affect the experimental results. Although detergent was generally dissolved in the original bead solution, the trace concentration of detergent in original bead solution was as low as ~0.1% provided by the manufacturer. After mixing bead with PBS, the final concentration was ~0.0002%, and considered to have negligible effect on NV formation.

3.6. Delivery of polystyrene bead encapsulated NVs

By using PS beads as representative of exogenous materials, the delivery ability of NVs was confirmed. MEF-GFP cells treated with bead-encapsulating NVs had more red fluorescent dots in their membranes than did the cells treated with bead-aggregated NVs (Fig. 7d). In addition, the cells treated with bare bead with equivalent fluorescent intensity of bead-encapsulating NVs showed no red dots in their membrane, although the beads <500 nm in diameter can be internalized by non-phagocytic cells [42]. These results implicate that materials to which the plasma membrane is impermeable can be delivered to cells by being encapsulated in the NVs.

4. Conclusion

NVs that can encapsulate and deliver exogenous materials were generated by passing cells through a cell-slicing microfluidic system-on-a-chip. The sliced plasma fragments self-assembled into NVs due the minimization of free energy of lipid bilayer. The number of particles produced was ~150 × 10^8 per million ES cells and their size was ~100–300 nm. Although the contents of the NVs were compared to ES cells and identified to be similar in terms of intracellular proteins, membrane proteins and intracellular RNAs

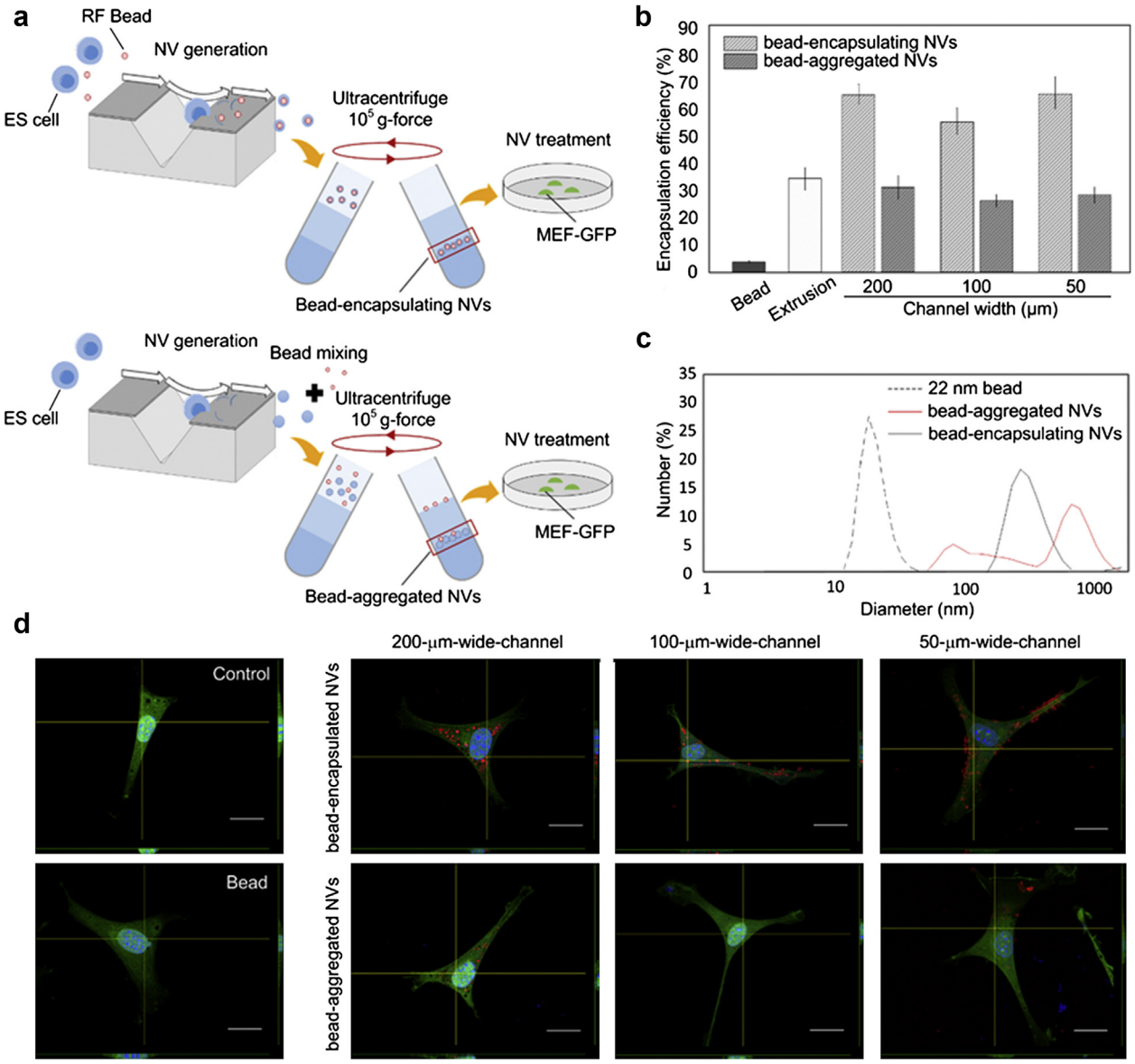

Fig. 7. Delivery of red fluorescent beads across the plasma membrane. (a) A schematics of the experiments. (b) Encapsulation efficiency of beads in NVs. Bead; unaided beads, Extrusion; bead-encapsulating NVs generated using centrifugal extrusion. The data were displayed mean ± S.D (n = 3). (c) Size distribution of three samples: 22 nm bead, bead-aggregated NVs, and bead-encapsulating NVs. (d) Confocal microscope images of MEF-GFP cells treated with bare beads and various NVs. Green: MEF-GFP, blue: Nucleus of MEF-GFP, Red: fluorescent bead. Scale bar = 20 μm. (For interpretation of the references to color in this figure legend, the reader is referred to the web version of this article.)

(mRNAs, small RNAs and rRNAs), NVs can also encapsulate fluorescent beads representing exogenous materials with ~30% encapsulation efficiency and deliver the encapsulated beads to recipient cells. Therefore, unlike cell-secreted exosomes, the NVs generated by the method introduced in this study can be used as vehicles for delivery of drugs and exogenous biomolecules.

Acknowledgments

This work was supported by the National Research Foundation of Korea (NRF) grant funded by the Korea government (MSIP) (No. 2011-0030075, 2011-0028845).

References

[1] L. Alvarez-Erviti, Y. Seow, H. Yin, C. Betts, S. Lakhal, M.J. Wood, Delivery of siRNA to the mouse brain by systemic injection of targeted exosomes, Nat Biotechnol 29 (4) (2011) 341–345.
[2] W. Perkins, S. Minchey, P. Ahl, A. Janoff, The determination of liposome captured volume, Chem Phys Lipids 64 (1) (1993) 197–217.
[3] E. Segura, C. Nicco, B. Lombard, P. Véron, G. Raposo, F. Batteux, et al., ICAM-1 on exosomes from mature dendritic cells is critical for efficient naive T-cell priming, Blood 106 (1) (2005) 216–223.
[4] C. Théry, S. Amigorena, G. Raposo, A. Clayton, Isolation and characterization of exosomes from cell culture supernatants and biological fluids, Curr Protoc Cell Biol (2006), 3.22. 1–3. 9.
[5] C. Théry, M. Ostrowski, E. Segura, Membrane vesicles as conveyors of immune responses, Nat Rev Immunol 9 (8) (2009) 581–593.
[6] A.J. Abusamra, Z. Zhong, X. Zheng, M. Li, T.E. Ichim, J.L. Chin, et al., Tumor exosomes expressing Fas ligand mediate CD8+ T-cell apoptosis, Blood Cells Mol Dis 35 (2) (2005) 169–173.
[7] W. Jo, J. Kim, J. Yoon, D. Jeong, S. Cho, H. Jeong, et al., Large-scale generation of cell-derived nanovesicles, Nanoscale 6 (20) (2014) 12056–12064.
[8] D. Jeong, W. Jo, J. Yoon, J. Kim, S. Gianchandani, Y.S. Gho, et al., Nanovesicles engineered from ES cells for enhanced cell proliferation, Biomaterials 35 (34) (2014) 9302–9310.
[9] K.-S. Park, K.-H. Choi, Y.-S. Kim, B.S. Hong, O.Y. Kim, J.H. Kim, et al., Outer membrane vesicles derived from *Escherichia coli* induce systemic inflammatory response syndrome, PLoS One 5 (6) (2010) e11334.

[10] H. Peinado, M. Alečković, S. Lavotshkin, I. Matei, B. Costa-Silva, G. Moreno-Bueno, et al., Melanoma exosomes educate bone marrow progenitor cells toward a pro-metastatic phenotype through MET, Nat Med 18 (6) (2012) 883–891.
[11] A.V. Vlassov, S. Magdaleno, R. Setterquist, R. Conrad, Exosomes: current knowledge of their composition, biological functions, and diagnostic and therapeutic potentials, Biochim Biophys Acta 1820 (7) (2012) 940–948.
[12] G. Van Niel, G. Raposo, C. Candalh, M. Boussac, R. Hershberg, N. Cerf–Bensussan, et al., Intestinal epithelial cells secrete exosome–like vesicles, Gastroenterology 121 (2) (2001) 337–349.
[13] B. Maherani, E. Arab-Tehrany, M.R. Mozafari, C. Gaiani, M. Linder, Liposomes: a review of manufacturing techniques and targeting strategies, Curr Nanosci 7 (3) (2011) 436–452.
[14] W. Helfrich, Stiffening of fluid membranes and entropy loss of membrane closure: two effects of thermal undulations, Eur Phys J B 1 (4) (1998) 481–489.
[15] E. Hernández-Zapata, L. Martínez-Balbuena, I. Santamaría-Holek, Thermodynamics and dynamics of the formation of spherical lipid vesicles, J Biol Phys 35 (3) (2009) 297–308.
[16] J.N. Israelachvili, D.J. Mitchell, B.W. Ninham, Theory of self-assembly of lipid bilayers and vesicles, Biochim Biophys Acta 470 (2) (1977) 185–201.
[17] E. Sackmann, Membrane bending energy concept of vesicle-and cell-shapes and shape-transitions, FEBS Lett 346 (1) (1994) 3–16.
[18] R.T. Davies, D. Kim, J. Park, Formation of liposomes using a 3D flow focusing microfluidic device with spatially patterned wettability by corona discharge, J Micromech Microeng 22 (5) (2012) 055003.
[19] A. Sharma, U.S. Sharma, Liposomes in drug delivery: progress and limitations, Int J Pharm 154 (2) (1997) 123–140.
[20] J.W. Park, Liposome-based drug delivery in breast cancer treatment, Breast Cancer Res 4 (3) (2002) 95.
[21] Y. Perrie, G. Gregoriadis, Liposome-entrapped plasmid DNA: characterisation studies, Biochim Biophys Acta Gen Subj 1475 (2) (2000) 125–132.
[22] J.J. Sudimack, W.J. Guo, W. Tjarks, R.J. Lee, A novel pH-sensitive liposome formulation containing oleyl alcohol, Biochim Biophys Acta Biomembr 1564 (1) (2002) 31–37.
[23] J.C. Stachowiak, D.L. Richmond, T.H. Li, A.P. Liu, S.H. Parekh, D.A. Fletcher, Unilamellar vesicle formation and encapsulation by microfluidic jetting, Proc Natl Acad Sci U S A 105 (12) (2008) 4697–4702.
[24] Y.-C. Tan, K. Hettiarachchi, M. Siu, Y.-R. Pan, A.P. Lee, Controlled microfluidic encapsulation of cells, proteins, and microbeads in lipid vesicles, J Am Chem Soc 128 (17) (2006) 5656–5658.
[25] A. Bangham, M.M. Standish, J. Watkins, Diffusion of univalent ions across the lamellae of swollen phospholipids, J Mol Biol 13 (1) (1965), 238–IN27.
[26] D. Deamer, A. Bangham, Large volume liposomes by an ether vaporization method, Biochim Biophys Acta 443 (3) (1976) 629–634.
[27] A. Jahn, W.N. Vreeland, D.L. DeVoe, L.E. Locascio, M. Gaitan, Microfluidic directed formation of liposomes of controlled size, Langmuir 23 (11) (2007) 6289–6293.
[28] F. Szoka, D. Papahadjopoulos, Procedure for preparation of liposomes with large internal aqueous space and high capture by reverse-phase evaporation, Proc Natl Acad Sci U S A 75 (9) (1978) 4194–4198.
[29] W. Jo, D. Jeong, J. Kim, S. Cho, S.C. Jang, C. Han, et al., Microfluidic fabrication of cell-derived nanovesicles as endogenous RNA carriers, Lab Chip 14 (7) (2014) 1261–1269.
[30] S.C. Jang, Y.S. Gho, Could bioengineered exosome-mimetic nanovesicles be an efficient strategy for the delivery of chemotherapeutics? Nanomedicine (Lond) 9 (2) (2014) 177–180.
[31] S.C. Jang, O.Y. Kim, C.M. Yoon, D.-S. Choi, T.-Y. Roh, J. Park, et al., Bioinspired exosome-mimetic nanovesicles for targeted delivery of chemotherapeutics to malignant tumors, ACS Nano 7 (9) (2013) 7698–7710.
[32] N. Sharma, M. Hooda, S. Sharma, Synthesis and characterization of LPCVD polysilicon and silicon nitride thin films for MEMS applications, J Mater (2014) 2014.
[33] M. Antonietti, S. Förster, Vesicles and liposomes: a self-assembly principle beyond lipids, Adv Mater 15 (16) (2003) 1323–1333.
[34] L.A. Meijer, F.A. Leermakers, J. Lyklema, Modeling the interactions between phospholipid bilayer membranes with and without additives, J Phys Chem U S 99 (47) (1995) 17282–17293.
[35] T. Le, U. Olsson, K. Mortensen, Topological transformation of a surfactant bilayer, Phys B 276 (2000) 379–380.
[36] J.B. Harford, Preparation and isolation of cells, Curr Protoc Cell Biol 32 (2006). John Wiley & Sons, Inc. [Chapter 2, 2.0.1-2.7.21].
[37] H. Jeong, T. Li, Y.B. Gianchandani, J. Park, High precision cell slicing by harmonically actuated ultra-sharp SixNy blades, J Micromech Microeng 25 (2) (2015) 025007.
[38] A. Savina, M. Furlán, M. Vidal, M.I. Colombo, Exosome release is regulated by a calcium-dependent mechanism in K562 cells, J Biol Chem 278 (22) (2003) 20083–20090.
[39] A. Montecalvo, A.T. Larregina, W.J. Shufesky, D.B. Stolz, M.L. Sullivan, J.M. Karlsson, et al., Mechanism of transfer of functional microRNAs between mouse dendritic cells via exosomes, Blood 119 (3) (2012) 756–766.
[40] L. Tian, J.W. Catt, C. O'Neill, N. King, Expression of immunoglobulin superfamily cell adhesion molecules on murine embryonic stem cells, Biol Reprod 57 (3) (1997) 561–568.
[41] P. Fairchild, F. Brook, R. Gardner, L. Graca, V. Strong, Y. Tone, et al., Directed differentiation of dendritic cells from mouse embryonic stem cells, Curr Biol 10 (23) (2000) 1515–1518.
[42] J. Rejman, V. Oberle, I.S. Zuhorn, D. Hoekstra, Size-dependent internalization of particles via the pathways of clathrin- and caveolae-mediated endocytosis, Biochem J 377 (Pt 1) (2004) 159–169.